

MIT Open Access Articles

Quantifying the impact of sulfate geoengineering on mortality from air quality and UV-B exposure

The MIT Faculty has made this article openly available. **Please share** how this access benefits you. Your story matters.

Citation: Eastham, Sebastian D. et al. "Quantifying the impact of sulfate geoengineering on mortality from air quality and UV-B exposure." *Atmospheric Environment* 187 (August 2018): 424-434 © 2018 Elsevier Ltd

As Published: <http://dx.doi.org/10.1016/j.atmosenv.2018.05.047>

Publisher: Elsevier BV

Persistent URL: <https://hdl.handle.net/1721.1/126693>

Version: Author's final manuscript: final author's manuscript post peer review, without publisher's formatting or copy editing

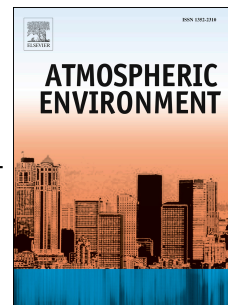
Terms of use: Creative Commons Attribution-NonCommercial-NoDerivs License



Accepted Manuscript

Quantifying the impact of sulfate geoengineering on mortality from air quality and UV-B exposure

Sebastian D. Eastham, Debra K. Weisenstein, David W. Keith, Steven R.H. Barrett



PII: S1352-2310(18)30351-0

DOI: [10.1016/j.atmosenv.2018.05.047](https://doi.org/10.1016/j.atmosenv.2018.05.047)

Reference: AEA 16038

To appear in: *Atmospheric Environment*

Received Date: 16 January 2018

Revised Date: 22 May 2018

Accepted Date: 23 May 2018

Please cite this article as: Eastham, S.D., Weisenstein, D.K., Keith, D.W., Barrett, S.R.H., Quantifying the impact of sulfate geoengineering on mortality from air quality and UV-B exposure, *Atmospheric Environment* (2018), doi: 10.1016/j.atmosenv.2018.05.047.

This is a PDF file of an unedited manuscript that has been accepted for publication. As a service to our customers we are providing this early version of the manuscript. The manuscript will undergo copyediting, typesetting, and review of the resulting proof before it is published in its final form. Please note that during the production process errors may be discovered which could affect the content, and all legal disclaimers that apply to the journal pertain.

1 **Quantifying the impact of sulfate geoengineering on mortality from air quality and**
2 **UV-B exposure**

3 **Sebastian D. Eastham^{a*}, Debra K. Weisenstein^b, David W. Keith^b, and Steven R. H.**
4 **Barrett^a**

5 ^a Laboratory for Aviation and the Environment, Department of Aeronautics and Astronautics,
6 Massachusetts Institute of Technology, Cambridge, MA 02139.

7 ^b School of Engineering and Applied Sciences, Harvard University, Cambridge, MA 02139.

8 *Corresponding author: Sebastian Eastham

9 E-mail: seastham@mit.edu

10 Telephone: +1 (617) 258-6347

11 Address: 77 Massachusetts Avenue, Cambridge, MA 02139

12 **Highlights:**

- 13 • Direct, non-climate effects of sulfate injection produce net health risk reduction
- 14 • Surface sulfur emission incurs 25 times the exposure from stratospheric injection
- 15 • Disbeneficial climate change-driven health effects dominate impacts of injection
- 16 • Net impacts of injection harmful despite beneficial photochemical response
- 17 • Injection health impacts small relative to risks associated with climate change

18 **Abstract**

19 Sulfate geoengineering is a proposed method to partially counteract the global radiative
20 forcing from accumulated greenhouse gases, potentially mitigating some impacts of climate
21 change. While likely to be effective in slowing increases in average temperatures and extreme
22 precipitation, there are known side-effects and potential unintended consequences which have
23 not been quantified. One such consequence is the direct human health impact. Given the
24 significant uncertainties, we take a sensitivity approach to explore the mechanisms and range of
25 potential impacts. Using a chemistry-transport model, we quantify the steady-state response of
26 three public health risks to 1°C global mean surface cooling. We separate impacts into those
27 which are “radiative forcing-driven”, associated with climate change “reversal” through
28 modification of global radiative forcing, and those “direct impacts” associated uniquely with
29 using sulfate geoengineering to achieve this. We find that the direct (non-radiative forcing
30 driven) impact is a decrease in global mortality of ~13,000 annually. Here the benefits of reduced
31 ozone exposure exceed increases in mortality due to UV and particulate matter, as each unit of
32 injected sulfur incurs 1/25th the particulate matter exposure of a unit of sulfur emitted from
33 surface sources. This reduction is exceeded by radiative forcing-driven health impacts resulting
34 from using sulfate geoengineering to offset 1°C of surface temperature rise. Increased particulate
35 matter formation at these lower temperatures results in ~39,000 mortalities which would have
36 been avoided at higher temperatures. As such we estimate that sulfate geoengineering in 2040
37 would cause ~26,000 (95% interval: -30,000 to +79,000) early deaths annually relative to the
38 same year without geoengineering, largely due to the loss of health benefits associated with CO₂-
39 induced warming. These results account only for impacts due to changes in air quality and UV-B
40 flux. They do not account for non-mortality impacts or changes in atmospheric dynamics, and

41 must be considered in the wider context of other climate change impacts such as heatwave
42 frequency and sea level rise.

43 **Keywords:** Geoengineering; air quality; UV exposure; ozone; mortality

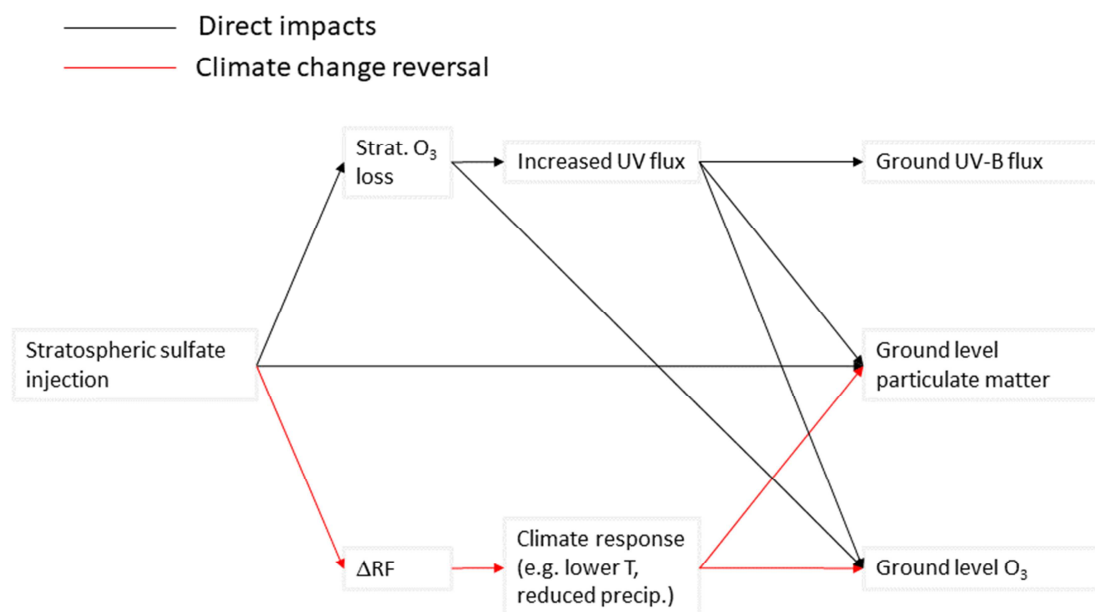
44 **1 Introduction**

45 Sulfate geoengineering is one of several possible forms of solar radiation management
46 (SRM), proposed as a method to reduce the net harm resulting from anthropogenic climate
47 change. By promoting the formation of a long-lived stratospheric aerosol layer, a fraction of
48 incoming solar radiation can be scattered back to space before it could be absorbed by the
49 atmosphere, partially offsetting the net anthropogenic radiative forcing. The efficacy of a natural
50 or artificial sulfate layer in reducing global temperature and precipitation has been widely
51 investigated. Early investigations focused on large volcanic eruptions, which are known to
52 produce transient stratospheric aerosol layers (*McCormick et al.*, 1995), while later climate
53 modeling studies explored the possible outcomes of sulfate geoengineering (*Rasch et al.*, 2008).
54 Although the climate and public health impacts of sulfate geoengineering have been discussed
55 (*NAS 1992, Pitari et al.*, 2014, *Effiong et al.*, 2016), to date there has not been a quantitative
56 evaluation of how global mortality rates might be affected by changes in air quality or UV-B
57 exposure resulting from such a strategy.

58 Air quality, specifically surface-level concentrations of ozone and fine particulate matter
59 ($PM_{2.5}$), has been linked quantitatively to changes in mortality rates through exposure response
60 functions based on epidemiological studies (*Hoek et al.*, 2014, *Jerrett et al.*, 2010). A similar
61 function has been developed for exposure to UV-B radiation, with the aim of estimating avoided
62 skin cancer incidence due to implementation of the Montreal protocol (*Slaper et al.*, 1996). The

63 existence of these functions allows the effect of any policy or technology on each of these factors
64 to be calculated and compared in common units. Degraded air quality is estimated to cause ~8%
65 of all global mortality in 2015 (Cohen *et al.*, 2017), and changes to air quality are frequently
66 considered in the context of climate change. A recent study found that mitigation of greenhouse
67 gas emissions from an “unconstrained” scenario down to those in the IPCC RCP4.5 scenario
68 would result in ~1.3 million fewer mortalities per year in 2050 due to both changes in climate
69 and the required changes in emissions (West *et al.*, 2013). This estimation technique has been
70 applied in source-specific impacts evaluations such as for aircraft emissions (e.g. Eastham and
71 Barrett, 2016), but has not yet been applied to an analysis of sulfate geoengineering.

72 The mechanisms by which an SRM proposal affects these outcomes can be separated into
73 two categories: the “direct” impacts of the method, and the “RF (radiative-forcing)-driven”
74 impacts. Figure 1 gives a conceptual overview of how these categories apply to the impact
75 pathways between stratospheric injection of sulfate aerosol and human health impacts. “Direct
76 impacts”, shown in black, include any effects of the technique which would occur even if there
77 were no effect on the climate. For sulfate geoengineering, an example would be the descent of
78 injected aerosol to the surface. Falling aerosol will add to the existing burden of near-surface fine
79 particulate matter, degrading surface air quality and incurring public health damages in the form
80 of increased respiratory disease mortality rates. This impact would occur regardless of whether
81 the injected aerosol successfully reduced the net radiative imbalance. A second example is the
82 effect of sulfate geoengineering on stratospheric ozone, and the resulting effect on the intensity
83 of surface-level UV-B radiation. Although this has been discussed in the literature in terms of
84 changes in mean intensity (Pitari *et al.*, 2014, Nowack *et al.*, 2016, Xia *et al.*, 2017), the impact
85 on human health has never been quantified.



86

87 Figure 1. Influence diagram for impacts of sulfate geoengineering on public health. Only first-order influences are shown here.

88 Minor contributions which may still be significant, such as the direct scattering effect of sulfate aerosols on surface UV-B flux,
89 are not shown for the sake of clarity.

90 “RF-driven” impacts, shown in Figure 1 in red, include only those which result from the
91 change in radiative forcing achieved by the injected aerosol. Although there are some ways in
92 which the effects of sulfate geoengineering are expected to differ from a simple reversal of
93 climate change (*Caldeira et al.*, 2013), RF-driven impacts are likely to be dominated by the
94 avoided effects of climate change. For example, increasing temperatures associated with climate
95 change are expected to increase ozone concentrations in polluted regions (*Fiore et al.*, 2012). By
96 mitigating future increases in temperature, sulfate geoengineering might reduce total mortality
97 due to ozone exposure relative to the avoided future scenario. Similarly, any potential localized
98 benefits of climate change such as increased crop yields in previously-unproductive regions
99 (*Reilly et al.*, 1994) would also be lost.

100 The relative contribution of each impact pathway to the total impact of sulfate
101 geoengineering depends on multiple uncertain quantities. Although volcanic events have
102 provided evidence that a stratospheric sulfate layer can provide a negative radiative forcing, the
103 total forcing achieved per unit mass injected varies between studies. For a given target outcome –
104 for example, a 1°C reduction in global average surface temperature – the required rate of sulfate
105 injection will depend on the lifetime and properties of the aerosol layer produced, in addition to
106 the sensitivity of the climate to an increase in stratospheric aerosol optical depth. There are large
107 differences in the estimates of the RF per unit sulfate, differences that depend, in part, on the way
108 sulfates are introduced to the stratosphere (*Pierce et al., 2010, Niemeier and Timmreck, 2015*).
109 The magnitude of these variables could affect the total impact of sulfate geoengineering, and the
110 contribution of each pathway. Lower RF per unit sulfate means larger direct impacts per unit
111 climate benefit. A world with a low climate sensitivity (the rate of change of temperature with
112 respect to aerosol optical depth, $\partial T/\partial\tau$) will require more injected mass to achieve the same
113 temperature reduction target than a world with a high climate sensitivity, but the amount of
114 temperature reduction used in a low-sensitivity world will presumably be correspondingly less.
115 Although temperature-related impacts would be unaffected, impacts directly related to the
116 presence of more stratospheric aerosol, including stratospheric ozone changes, and therefore
117 UV-B exposure, will be greater for the former case than the latter. Although a spot estimate of
118 geoengineering's impacts on global mortality can be achieved in a single model run, a more
119 nuanced approach is required to understand what the contribution of each pathway is to the total,
120 and how these contributions are affected by uncertainty in input parameters such as climate
121 sensitivity.

122 We use a global chemistry-transport model (CTM) to compute the response of air quality
123 and population UV-B exposure to sulfate geoengineering at a rate of 1 TgS/yr, isolating the
124 direct and RF-driven impacts using a hybrid modeling approach. Direct impacts of sulfate
125 geoengineering are estimated using offline CTM simulations, in which meteorological fields are
126 specified and no climate response is simulated. RF-driven impacts are estimated by re-running
127 the CTM with perturbed meteorological fields, using a GCM to calculate temperature and
128 precipitation changes resulting from sulfate geoengineering. For each of these simulations, the
129 impact of the relevant pathway is calculated by comparison to a baseline simulation in which no
130 sulfate geoengineering is simulated. Assuming a linear relationship of uncertain slope between
131 stratospheric AOD and temperature change, we apply a Monte-Carlo method to estimate the
132 overall impact of sulfate geoengineering sufficient to achieve a 1°C reduction in global average
133 surface temperature on global mortality due to air quality and UV-B exposure, quantifying the
134 contribution of direct and RF-driven impact pathways to the total.

135 **2 Methods**

136 Air quality and UV-B exposure changes resulting from sulfate geoengineering are
137 calculated using a hybrid modeling approach, combining simulations in a global chemistry-
138 transport model (CTM) with results from a sulfate geoengineering simulation in a global climate
139 model (GCM). For each scenario, impacts are calculated by calculating the difference in results
140 between the output from two CTM simulations.

141 CTM simulations are performed using prescribed meteorology, so climate feedbacks are
142 decoupled from the atmospheric conditions in the model. RF-driven impacts are simulated by
143 imposing pre-calculated changes in temperature and precipitation directly to the meteorological
144 fields within the CTM. This allows the direct and RF-driven impacts to be isolated, while taking

145 advantage of the modeling skill of the CTM's chemical mechanism with respect to simulating
146 changes in air quality and UV-B exposure. The properties of stratospheric aerosol under baseline
147 and geoengineered conditions are also calculated separately, using a dedicated aerosol
148 microphysics model to provide size parameters for each case. The model setup to simulate
149 atmospheric composition in 2040 with and without sulfate geoengineering, and the approach
150 used to disaggregate impact pathways, is described in section 2.1.

151 These CTM simulations are sufficient to provide a single estimate of the net impact of
152 geoengineering at a rate of 1 TgS/yr on surface air quality and UV-B exposure, in addition to the
153 relative contribution of each direct and RF-driven impact to the total. However, it does not
154 account for uncertainty in the climatological response. By assuming linearity in the relationships
155 between several atmospheric and climatological variables, we convert our estimate of the impact
156 of 1 TgS/yr of aerosol injection into the impact of a specific target climate outcome: offsetting
157 1°C of global mean surface temperature increase. This method is described in section 2.2.

158 We also extrapolate the effect of uncertainty in the climate variables to compute the level
159 of uncertainty in the net impact of sulfate geoengineering on air quality and UV-B, holding the
160 target climate outcome constant. The Monte-Carlo method applied to achieve this is described in
161 section 2.3. Finally, we apply epidemiological exposure-response functions to determine the net
162 change in global mortality resulting from achieving this climate outcome, and the relative
163 contribution of direct and RF-driven mechanisms. This is described in section 2.4.

164 2.1 Atmospheric modeling

165 Impacts of sulfate geoengineering are computed for a target year of 2040. Atmospheric
166 composition in 2040, with and without sulfate geoengineering and the associated RF-driven
167 impacts, is calculated using the GEOS-Chem atmospheric model.

168 GEOS-Chem is a global chemistry-transport model (CTM), directly simulating
169 atmospheric chemistry, transport, radiative transfer of UV, emissions, and loss processes.
170 Following the recent implementation of a unified tropospheric-stratospheric chemistry extension,
171 GEOS-Chem uses the same comprehensive chemical mechanism throughout both the
172 troposphere and stratosphere, including an explicit representation of stratospheric aerosols
173 (*Eastham et al.*, 2014). For all CTM simulations we use meteorological fields produced from the
174 NASA GMAO Global Earth Observation System (GEOS-5) for the years 2004-2010. This
175 simulation period is repeated once to yield 14 years of output. The meteorological data is made
176 up of 72 layers from the surface to 0.1 hPa, and is regridded to a horizontal resolution of $4^{\circ} \times 5^{\circ}$.
177 Boundary conditions and surface anthropogenic emissions are taken from the RCP 4.5 projection
178 for 2040 (*Wise et al.*, 2009, *Clarke et al.*, 2007, *Smith et al.*, 2006). Initial conditions
179 representative of the future atmosphere are calculated using a prior 14-year spinup simulation,
180 resulting in a total integration time of 28 years. This extended integration time is required to
181 ensure that the model has reached steady state prior to the period of analysis. The effects of
182 geoengineering are calculated by comparing the mean atmospheric state over the final five years
183 between two simulations (e.g. the results of a simulation with 1 TgS/yr injection are compared to
184 a baseline simulation in which no sulfate geoengineering is employed). Surface-level $PM_{2.5}$ and
185 ozone concentrations are retrieved based on the output at the lowest model layer. UV-B exposure
186 is calculated based on the surface-level incident UV radiation fluxes estimated by the Fast-JX

187 UV radiative transfer and photolysis code embedded in GEOS-Chem, with each wavelength bin
188 weighted according to the SCUP-h action spectrum relevant to UV-induced DNA damage in
189 human skin (*de Gruijl and Van der Leun, 1994*).

190 The microphysical properties of the stratospheric aerosol are estimated separately, using
191 the AER 2-D microphysical model (*Weisenstein et al., 1997, 2007*). Based on the results of these
192 simulations, a log-normal size distribution is estimated and applied to all sulfate-based
193 stratospheric aerosol in the CTM. For baseline conditions, a modal radius of 0.06 μm is used.
194 More details are given in the SI.

195 We simulate sulfate geoengineering by directly emitting aerosol into the stratosphere.
196 Sulfate is injected at a rate of 1 TgS/yr between 20 and 25 km pressure altitude, from 30°S to
197 30°N, and over all longitudes. Consistent with the findings of Pierce et al. (2010) and Benduhn et
198 al. (2016), we assume that sulfur is emitted directly as a sulfate aerosol with the target
199 microphysical properties, rather than as SO₂. Based on results from a 1 TgS/yr injection
200 simulation with the microphysical model we impose a log-normal size distribution on the
201 geoengineered aerosol with a modal radius of 0.16 μm , approximately 2.7 times larger (by
202 radius) than under the baseline case. In an initial calibration simulation, we found that this
203 injection rate results in a mean stratospheric aerosol optical depth (AOD) of 0.079, and that the
204 monthly-average stratospheric burden of geoengineering-attributable sulfate varies by less than
205 $\pm 3\%$ over the five years used to calculate the mean atmospheric state. This approach is sufficient
206 to capture direct impacts of sulfate geoengineering in the absence of the climate response.
207 However, capturing RF-driven impacts requires that the climate response to sulfate
208 geoengineering is simulated or imposed within the CTM.

209 The response of climate variables (e.g. temperature) to sulfate geoengineering is not
210 coupled to atmospheric composition in the CTM. Instead, temperature and precipitation changes
211 are estimated based on GCM results from GeoMIP (*Kravitz et al., 2013*). In GeoMIP experiment
212 G4, CanESM2 estimated the climate response to a 0.0472 increase in global stratospheric AOD.
213 We took the gridded, monthly mean output fields from this simulation and normalized them by
214 the change in AOD to estimate the temperature response per unit change in the stratospheric-
215 average AOD ($\partial T_{3D}/\partial \tau$). The scalar rate of change of global precipitation per unit change in
216 global average surface temperature ($\partial P/\partial T_{sfc}$) was also estimated. These sensitivities are scaled
217 by the mean change in AOD from the calibration simulation to provide an estimate of the change
218 in temperature and precipitation resulting from sulfate geoengineering at a rate of 1 TgS/yr.
219 These changes are then applied to the meteorological fields within the CTM to estimate the RF-
220 driven impacts of sulfate geoengineering on air quality and UV-B exposure. Changes in
221 temperature are applied as a 3-D, absolute change in the temperature field, while changes in
222 precipitation are applied as a relative change in the global average precipitation rate. In both
223 cases, seasonal variation is captured by using monthly mean values rather than an annual
224 average. Further information is provided in the SI.

225

226 2.2 Calculation of impacts for a fixed injection rate

227 As described at the start of section 2, we first calculate the total impact of sulfate
 228 injection at a rate of 1 TgS/yr, and separate these impacts into direct and RF-driven pathways. To
 229 achieve this, we run 6 separate GEOS-Chem simulations, shown in Table 1.

230 Table 1. Simulation parameters used for each GEOS-Chem model run.

Simulation	Sulfate injection	Precipitation adjustment	Temperature adjustment	Chemistry
Baseline (B)	-	-	-	Yes
Calibration (O)	Yes	-	-	Yes
Central (C)	Yes	Yes	Yes	Yes
Precipitation sensitivity (S_P)	Yes	-	Yes	Yes
Temperature sensitivity (S_T)	Yes	Yes	-	Yes
Inert aerosol (I)	Yes	-	-	-

231 The net impact of 1 TgS/yr of sulfate geoengineering on air quality and UV-B exposure
 232 is estimated by subtracting the results of the baseline simulation (B) from those of the central
 233 simulation (C). The exposure resulting from all emissions in a given scenario (e.g. scenario S)
 234 can be represented as $E(S)$, such that the change in exposure due to all effects combined is $E(C)$
 235 $- E(B)$. In the central simulation, all impact pathways are simulated together. 1 TgS/yr of aerosol
 236 is injected. Air temperatures are decreased relative to the baseline simulation according to the
 237 pre-calculated temperature sensitivity field described in section 1.1, scaled by the 0.079
 238 stratospheric AOD estimated from the calibration simulation. Global precipitation is also
 239 decreased relative to the baseline. Post-simulation analysis of the simulation C showed a
 240 stratospheric AOD increase of 0.075, within 6% of the value used for calibration.

241 The contribution of direct (non-RF) pathways to the total impact of sulfate
242 geoengineering is estimated using results from the calibration simulation (0). Specifically, the
243 total contribution of direct pathways (all black arrows in Figure 1) to the net impact of sulfate
244 geoengineering on air quality and UV-B exposure is calculated by subtracting the “RF-driven”
245 impact from the total impact, as $[E(C) - E(B)] - [E(C) - E(0)]$. This is equivalent to $E(0) - E(B)$
246 and does not account for second-order terms resulting from, for example, the effect of changes in
247 precipitation on the direct pathways. However, these terms are quantified in Appendix B and
248 found to be negligible.

249 The contribution of each of the RF-driven pathways to the total is isolated by performing
250 two sensitivity simulations. Each is identical to simulation C, but without one of the two climate
251 perturbations. For example, in simulation S_T , sulfate aerosol is injected and global precipitation
252 is reduced, but temperatures are left unperturbed relative to the baseline. The difference in air
253 quality and UV-B impacts between simulation S_T and simulation C, calculated as (for example)
254 $E(C) - E(S_T)$, provides an estimate of the contribution of temperature change (an RF-driven
255 impact) to the net impact of sulfate geoengineering. We refer to the contribution of each of the
256 two RF-driven pathways as the “offset warming” and “offset precipitation” impacts, on the basis
257 that these changes are offsetting impacts of climate change. These pathways account for the
258 effect that the geoengineering-attributable change in RF, and therefore the change in climate, has
259 on background air quality and UV-B exposure. Again, cross terms resulting from interaction
260 between temperature- and precipitation- driven impacts are quantified in Appendix B and found
261 to be negligible.

262 We run one additional simulation to better disaggregate the direct (non-RF-driven)
263 pathways. The contribution of descending injected sulfate aerosol to concentrations of fine

264 particulate matter at the surface is calculated by performing a separate simulation, without
265 temperature or precipitation perturbations, in which a chemically unreactive aerosol is injected
266 (simulation I). This aerosol undergoes the same loss mechanisms as sulfate aerosol. This direct
267 impact pathway is referred to as the “descending aerosol” pathway. The net impact due to
268 descending aerosol is simply $E(I)$, as no other aerosol emissions or formation pathways are
269 included in this simulation.

270 Any changes in air quality and UV-B exposure observed in simulation 0 which are not
271 present in this inert simulation are assumed to be the photochemical response of the atmosphere
272 to the increased stratospheric loading, calculated as $[E(0) - E(B)] - E(I)$. This direct impact
273 pathway is referred to as the “photochemical” pathway. Specifically, this is the contribution of
274 photochemical processes to the total impact of sulfate geoengineering after the impacts of RF
275 changes on background air quality and UV-B exposure have been accounted for.

276 2.3 Impacts and uncertainty quantification for a fixed target warming offset

277 The combination of simulations listed in Table 1 provides an estimate of how sulfate
278 geoengineering at a rate of 1 TgS/yr would impact air quality and UV-B exposure, in addition to
279 the contribution from each of four direct and RF-driven pathways. Based on the mean climate
280 sensitivity from CanESM2 and the calculated stratospheric AOD from GEOS-Chem, this is also
281 the impact of sulfate geoengineering sufficient to offset 1°C of warming. By assuming linearity
282 in the atmospheric response, these same results can be used to answer a different question: the
283 contribution of uncertainty in the atmospheric response to both the total impact and the
284 contributions of each pathway.

285 We use a Monte-Carlo approach to explore how uncertainty in three climate variables
286 (Table 2) affects the total calculated change in air quality and UV-B exposure, holding constant
287 the target of offsetting 1°C of surface warming. We assume a linear relationship for each of the
288 following pairs of variables, with the slope of each relationship treated as an uncertain variable:
289 between injection rate and stratospheric aerosol burden (the aerosol lifetime); between
290 stratospheric AOD and temperature change (the climate sensitivity); and between temperature
291 change and precipitation change (the hydrological sensitivity). In each Monte-Carlo simulation,
292 an independent draw of these three variables is taken, and the total impact is recalculated by re-
293 weighting the contribution from each of the four pathways.

294 We assume that a reduction in the hydrological sensitivity will result in a proportional
295 reduction in impacts due to the RF-driven “offset precipitation” pathway. We assume that a
296 reduction in the climate sensitivity will result in a proportional increase in impacts due to the
297 direct impacts, on the assumption that a decreased climate sensitivity implies an increased AOD
298 for the same warming target, and therefore an increased injection rate. Finally, we assume that a
299 decreased aerosol lifetime implies an increase in the direct “descending aerosol” pathway only.
300 This is on the basis that decreased aerosol lifetimes imply an increased injection rate, but the
301 same overall AOD, with no effect on the overall RF achieved.

302 In each uncertain draw, aerosol lifetime is chosen based on a uniform distribution
303 between 1 and 2.4 years. This range spans most published estimates (*Heckendorn et al.*, 2009,
304 *Pierce et al.*, 2010, *Rasch et al.*, 2008) and includes the lifetime of 2.4 years simulated by
305 GEOS-Chem in the calibration scenario. For the climate and hydrological sensitivity parameters,
306 a value is randomly chosen from a set of four GeoMIP experiment G4 simulations with different

307 climate models (CanESM2, MIROC-ESM-CHEM, BNU-ESM and GISS-ER-2) (*Kravitz et al.*,
308 2013). The parameter distributions are shown in detail in Table 2.

309 Table 2. Uncertain parameters applied in Monte-Carlo simulations when converting simulation output to mortality estimates.
310 Triangular distributions are shown as the mode and 95% bounds. Limits of the distribution consistent with the 95% bounds were
311 calculated at simulation time. The “discrete” distribution corresponds to random selection of one of the listed values, taken from
312 the results of 4 models running the GeoMIP G4 simulations. T denotes temperatures; τ denotes stratospheric AOD; P denotes
313 global mean precipitation rate; M denotes number of premature mortalities; χ denotes population-weighted concentration.

Parameter	Distribution
Global temperature sensitivity ($\partial T/\partial \tau$) (K)	Discrete [-7.2, -7.3, -12, -19]
Global hydrological sensitivity ($\partial P/\partial T$) (% K^{-1})	Discrete [1.7, 2.4, 2.6, 2.9]
Mean stratospheric aerosol lifetime (years)	Uniform [1.0 – 2.4]
Ozone health response ($dM/d\chi$) (% ppbv ⁻¹)	Triangular [0.100 – 0.104 – 0.107]
PM _{2.5} health response ($dM/d\chi$) (% ($\mu g m^{-3}$) ⁻¹)	Triangular [0.500 – 1.10 – 1.60]
UV-B health response dose factor (unitless)	Triangular [0.2 – 0.6 – 1.0]

314

315 This process is described in more detail in the SI, and an assessment of the accuracy of
316 the linearity assumption is performed in Appendices A and B. Changes in second order effects
317 such as climate variability and atmospheric dynamics, which may affect cross-tropopause mass
318 flux and surface-level stagnation, are not modeled but are a clear priority for future work.

319 One potentially significant feedback which is not considered here is the effect of sulfate
320 geoengineering on cloud formation and properties. The increase in cloud condensation nuclei
321 (CCN) and ice nuclei resulting from the descent of emitted fine aerosol into the upper
322 troposphere could result in increased cirrus cloud formation, an effect which by one estimate

323 could contribute up to 60% of the net radiative forcing due to sulfate geoengineering (*Kuebbler,*
324 *Lohmann, and Feichter, 2012*). It is also possible that warm cloud formation could be affected by
325 the increase in CCN. Although this is not likely to be significant for this study, in which the
326 maximum injection rate considered is ~5-10% of current anthropogenic sulfur emissions (*Smith*
327 *et al., 2011*), scenarios involving higher rates of sulfate geoengineering emissions could result in
328 additional changes to precipitation patterns, intensity, and frequency which could significantly
329 affect surface concentrations of PM_{2.5}. Changes in cloud cover would also affect surface UV-B
330 intensity, potentially mitigating the skin cancer damages simulated here.

331 2.4 Calculation of health impacts

332 Once the total change in air quality and UV-B exposure for a given uncertain draw has
333 been computed, we convert the simulated changes in population exposure into an estimate of
334 global mortality. The gradients of the exposure response functions (ERFs), which reflect the
335 sensitivity of health outcomes to population exposure, are treated as uncertain variables, with
336 distributions described in Table 2. We use the non-linear Jerrett et al. (2009), Hoek et al. (2013)
337 and Slaper et al. (1996) ERFs for ozone, PM_{2.5} and UV-B exposure respectively. The Hoek ERF
338 was chosen for PM_{2.5} over the more common Krewski et al. (2009) ERF as it is a global meta-
339 analysis of epidemiological studies including Asia, whereas the latter is an in-depth
340 epidemiological study of the USA only. The effect of applying widely-used alternative ERFs for
341 PM_{2.5} such as those of Krewski or Burnett et al. (2014) is quantified, as is the effect of applying
342 concentration thresholds for both PM_{2.5} and ozone.

343 One thousand draws are performed for all six uncertain variables, using the Sobol
344 pseudo-random sampling sequence to improve convergence. Sensitivity of the results to each
345 input is calculated using the first-order contributions to total variance. This provides an estimate

346 of the first-order sensitivity indices (Sobol indices), corresponding to the fractional contributions
347 of uncertainty in each input to the total variance in the output (*Saltelli et al.*, 2008).

348 Two additional scenarios are simulated with alternative assumptions. The first applies
349 region-specific factors to precipitation changes to quantify the relative importance of global and
350 regional precipitation changes in calculating mortality. The second models a hypothetical low-
351 halogen future to account for the relative contributions of anthropogenic halogens in sulfate
352 geoengineering impact calculations (*Tilmes et al.*, 2009, *Tilmes et al.*, 2012, *Heckendorn et al.*,
353 2009). A full description of the approach used for these simulations is given in the SI.

354 **3 Results**

355 Impacts of implementing sulfate geoengineering sufficient to offset 1°C of surface
356 warming in 2040 are presented below. Direct pathways are discussed first, followed by RF-
357 driven pathways. A summary of the total impacts is provided in the Discussion section. In each
358 case, the calculated change in mortality is the result of the full Monte-Carlo simulation,
359 propagating uncertainty in climate sensitivity, aerosol microphysics, and exposure response. All
360 impacts are calculated for a projected global population in 2040 of 9 billion people (*United*
361 *Nations*, 2013)

362 **3.1 Direct impacts**

363 The first of the direct impacts considered is the descent of injected aerosol to the surface,
364 increasing the surface-level concentration of PM_{2.5}. We find that this pathway results in an
365 additional 7,400 premature mortalities per year due to degraded air quality (95% interval: 2,300
366 to 16,000). This implies that injection of aerosol into the stratosphere sufficient to offset 1°C of
367 surface warming would result in a net increase in mortality of the same order of magnitude as

368 attributable to jet fuel sulfur in 2006 (*Barrett et al.*, 2012), and an order of magnitude lower than
369 the impacts attributable to shipping in 2002 (*Corbett et al.*, 2007). In an additional sensitivity
370 simulation, we simulated continuous emission of an equal mass of aerosol at the surface,
371 distributed according to present-day surface-level sulfur emitters. Per unit mass emitted, we find
372 that surface-level emissions of sulfate result in 25 times greater population exposure to $PM_{2.5}$
373 than results from emitting the same aerosol into the stratosphere, while achieving a greater
374 radiative forcing offset due to the longer lifetime of stratospheric aerosol.

375 Direct photochemical changes, excluding the impact of injected aerosol descending to the
376 surface, is net negative, with a mean outcome of -42,000 premature mortalities per year (95%
377 interval: -42,000 to -4,900). This response is dominated by decreased ozone exposure at the
378 surface. Enhanced stratospheric ozone depletion results in reduced ozone mixing ratios in
379 surface-bound stratospheric air masses, while the increased mid-tropospheric flux of UV
380 radiation reduces the photochemical steady-state concentration of ozone throughout the
381 troposphere (*Zhang et al.*, 2014). Changes in the atmospheric dynamics, including the
382 stratosphere-troposphere ozone exchange rate due to dynamical effects of sulfate
383 geoengineering, are not considered but may affect this result (*Kirtman et al.*, 2014). The mean
384 change in global mortality due to reduced ozone exposure in this pathway is -23,000, exceeding
385 the mean increase in skin cancer mortality of 4,100 due to increased UV-B exposure. The
386 reduction in ozone also prompts a small decrease in $PM_{2.5}$, resulting in -1,400 premature
387 mortalities (-2,400 to -520) per year. This suggests that a small depletion in stratospheric ozone
388 may result in a net reduction in global mortality. This is a surprising result, and implies that
389 future increases in stratospheric ozone such as those projected under some climate change
390 scenarios (*Li et al.*, 2009) might be considered as a public health threat. However, this outcome

391 may be specific to the circumstances of the stratospheric ozone loss, and warrants further
392 research.

393 Previous studies have shown that the stratospheric ozone loss due to sulfate
394 geoengineering is sensitive to the assumed halogen loading, with one study even finding a
395 reversal of sign (*Tilmes et al., 2009, Tilmes et al., 2012, Heckendorn et al., 2009*). We simulate
396 an alternative scenario which corresponds to the theoretical minimum atmospheric halogen
397 loading. In this scenario all anthropogenic halogen emissions are set to zero, as are the initial
398 concentrations for all long-lived anthropogenic halogen gases (see SI for details). We find that
399 total ozone column depletion is reduced by 31% relative to the scenario with RCP 4.5 halogen
400 emissions, resulting in 2,500 fewer premature mortalities due to skin cancer, and 4,800 fewer due
401 to PM_{2.5} exposure. These benefits are exceeded by the increased ozone exposure in this scenario,
402 resulting in 7,600 additional mortalities. The net result is that the reduction in global mortality
403 due to direct photochemical impacts alone is smaller in magnitude by 3.6% under a low-halogen
404 scenario, relative to the baseline scenario. This again suggests that a relative increase in ozone
405 concentrations may have a net public health disbenefit, considering only air quality and UV-B
406 exposure.

407 Considering only direct impact pathways, sulfate geoengineering sufficient to offset 1°C
408 of surface warming results in a net benefit, with a global change of -13,000 premature mortalities
409 per year (sum of central estimates). Although we find 7,400 (2,300 to 16,000) additional
410 premature mortalities due to direct population exposure to injected aerosol, this is counteracted
411 by -20,000 (-42,000 to -4,900) premature mortalities due to photochemical impacts resulting
412 from the increased sulfur loading of the stratospheric aerosol layer.

413 3.2 RF-driven impacts

414 The calculated RF-driven impacts of sulfate geoengineering on air quality are consistent
415 with prior literature examining the related problem of the response of air quality to CO₂-driven
416 warming. Reduced temperatures relative to the projected future scenario result in enhanced
417 partitioning of HNO₃ from background emissions into nitrate aerosol, and therefore an increase
418 in surface PM_{2.5}. We find that this dominates other PM_{2.5} formation mechanisms which reduce in
419 response to cooler surface temperatures, such as production of biogenic aerosols. The result is
420 that, by offsetting 1°C of surface warming from climate change, sulfate geoengineering results in
421 an additional 69,000 premature mortalities annually (41,000 to 95,000). This increase is
422 accompanied by a significant decrease in premature mortality due to the avoided effect of global
423 warming on ozone. Ozone concentrations in polluted regions decrease with temperature as
424 photochemical production is slowed, such that sulfate geoengineering results in -43,000 (-67,000
425 to -19,000) premature mortalities per year due to ozone exposure relative to the avoided future.
426 The effect of temperature change on UV-B exposure is negligible.

427 The other RF-driven impact of sulfate geoengineering is lower overall precipitation rates,
428 offsetting some of the increased precipitation projected to result from climate change. Decreased
429 precipitation results in longer lifetimes for PM_{2.5} and therefore in increased PM_{2.5} exposure
430 globally. The total RF-driven impact of changes in precipitation from sulfate geoengineering is
431 an additional 14,000 (7,100 to 21,000) premature mortalities per year, with negligible effects on
432 ozone and UV-B exposure.

433 This approach assumes that precipitation will be uniformly affected across all locations,
434 and all aggregated impacts in the following sections are calculated on this assumption. However,
435 sulfate geoengineering is likely to reduce precipitation by a greater proportion in some regions

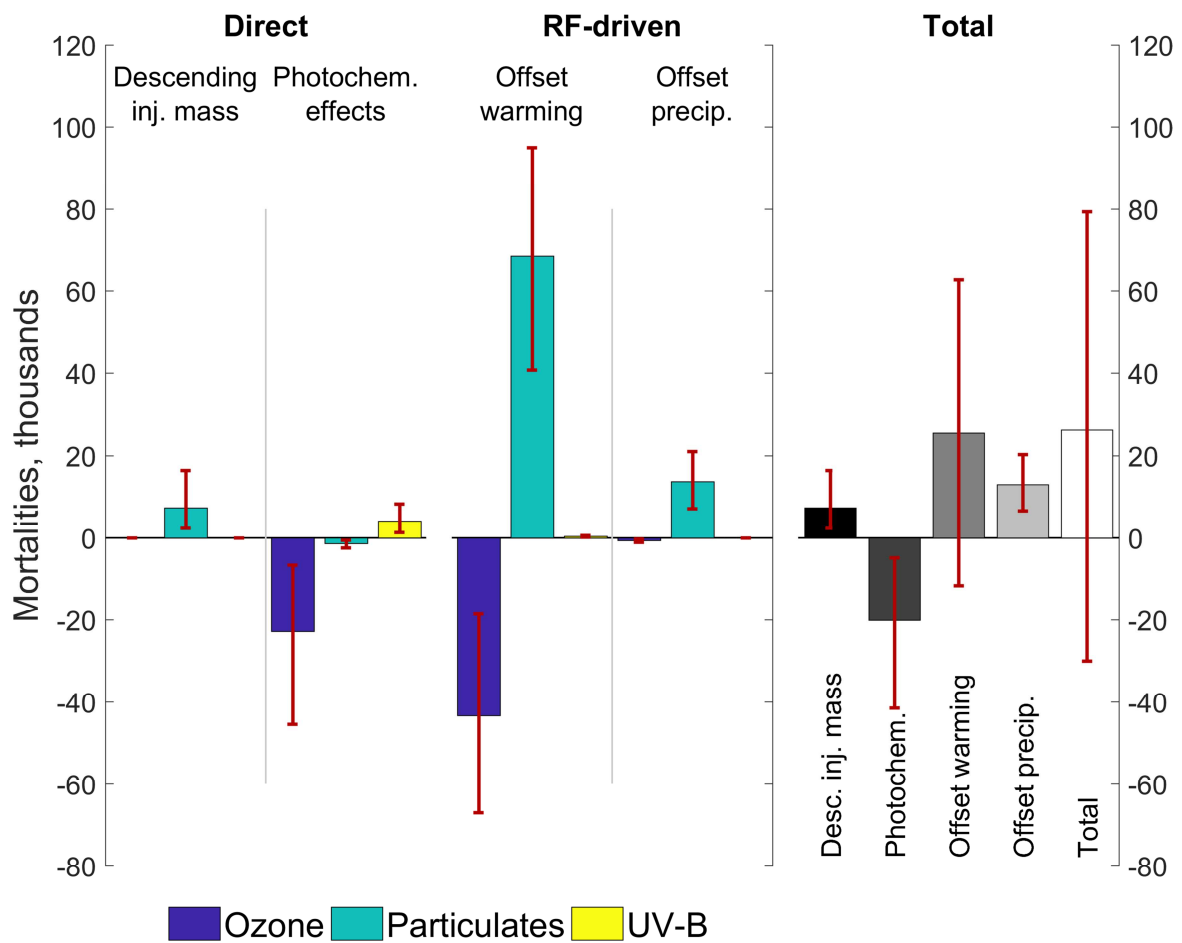
436 than in others (*Kravitz et al.*, 2014). We run an additional, sensitivity simulation in which
437 precipitation rate modifications are derived and applied on a local basis rather than a global
438 basis, using a separate factor derived from the GeoMIP G4 CanESM2 simulation for each of 21
439 climatologically-distinct regions (see SI for details). In this scenario, the impacts of precipitation
440 are increased by 15%. The increase occurs almost exclusively in Asia and Eastern Europe. Here
441 the relative reduction in precipitation is 1.5 and 4.5 times the global average, respectively,
442 resulting in longer lifetimes for $PM_{2.5}$ as washout is decreased. However, whether using global or
443 regional precipitation adjustments, impacts due to temperature change remain dominant factor in
444 RF-driven mortality impact pathways of sulfate geoengineering.

445 The net effect of RF-driven impact pathways on global air-quality and UV-B exposure is
446 a net increase in mortality, reflecting the loss of climate change-driven air quality benefits
447 associated with increasing temperature and precipitation. We find a combined central estimate of
448 39,000 additional mortalities per year due to this offsetting. This total is made up of +26,000
449 (-12,000 to +63,000) premature mortalities due to avoided temperature change, and +13,000
450 (+6,600 to +20,000) due to precipitation reduction.

451 These results are sensitive to the modeled impact of climate change on surface air quality.
452 We find that, for both RF-driven pathways, sulfate geoengineering offsets climate change-related
453 increases in ozone and decreases in $PM_{2.5}$, with the magnitude of mortality impacts from the
454 latter change exceeding those from the former. While increases of ozone under climate change
455 are widely reported in the literature, the sign of the impact of climate change on surface $PM_{2.5}$
456 concentrations is uncertain (*Fiore et al.*, 2012). The net outcome of RF-driven impacts is likely to
457 change as our understanding of the impacts of climate change is further refined.

458 **4 Discussion**

459 In total, and considering only the effects on air quality and UV-B exposure, sulfate
460 geoengineering sufficient to offset 1°C of warming results in +26,000 premature mortalities
461 annually (95% confidence interval of -30,000 to +79,000). Figure 2 shows a graphical
462 breakdown of incurred mortalities by pathway and by exposure type, with numerical values
463 shown in Table 3. This total is made up of 39,000 additional mortalities due to RF-driven
464 pathways, partially offset by 26,000 prevented mortalities due to direct pathways, as outlined in
465 Figure 1. In 17% of cases, mortality reductions due to decreased ozone exposure exceed the
466 combined global mortality impacts of increased PM_{2.5} and UV-B exposure, resulting in a net
467 decrease in global mortality due to sulfate geoengineering. Overall, surface air quality and skin
468 cancer impacts are dominated by increases in mortality due to RF-driven pathways, whereas the
469 direct impact pathways of sulfate geoengineering are net beneficial by these metrics.



470

471 Figure 2. Annual premature mortality impacts resulting from sulfate geoeengineering sufficient to offset 1°C of surface warming.

472 Impacts are separated by pathway, based on Figure 1, and by exposure type. The left panel shows the contributions to each

473 pathway's total impact, separated by exposure type. The right hand sub-plot shows how each impact pathway contributes to the

474 total. "Descending inj. mass" corresponds to direct exposure of the population to injected aerosol mass as it descends to the

475 surface. "Photochem. effects" corresponds to photochemical changes resulting from the increased aerosol optical depth and

476 surface area, including induced changes in stratospheric ozone columns. "Offset warming" corresponds to temperature change,

477 "Offset precip." to reductions in precipitation. Solid bars show the mean value of Monte Carlo simulation outcomes (n = 1,000).

478 Error bars show the 2.5 and 97.5th percentile values.

479 For all four atmospheric mechanisms, mortality due to surface ozone exposure is

480 consistently decreased by sulfate geoeengineering, whereas mortality due to PM_{2.5} exposure varies

481 in sign. Increases in nitrate aerosol due to reduced surface warming result, on average, in greater

482 health impacts than the benefits associated with reduced ozone. UV-B exposure is only
483 significantly affected by direct photochemical effects of sulfate geoengineering, but the
484 contribution of changes in UV-B exposure to the overall impact of sulfate geoengineering is an
485 order of magnitude smaller than the contributions of changes in ozone or PM_{2.5} exposure.

486 When considering only the direct photochemical consequences of sulfate geoengineering,
487 the total skin cancer mortality increase is exceeded by the ozone mortality decrease in all
488 uncertain variable draws. This counterintuitively implies that limited stratospheric ozone
489 destruction may be of net benefit in terms of premature mortality and human lifespan, and that
490 reduction of anthropogenic halogen emissions may increase rather than reduce health impacts
491 due to sulfate geoengineering. However, this does not take into account non-mortality outcomes
492 of exposure to UV-B such as cataract formation and non-melanoma skin cancer, which is less
493 fatal but several orders of magnitude more common than melanoma skin cancer (*Guy et al.*,
494 2015, *Slaper et al.*, 1996).

495 Uncertainty in the ERFs for PM_{2.5} and ozone have the greatest first-order effect on
496 overall variance in the global mortality impact of sulfate geoengineering, contributing 44% and
497 50% of the total variance in the result based on the calculated sensitivity indices. The first-order
498 effects of uncertainty in climate response are an order of magnitude smaller, with the greatest
499 contribution being 2.5% for temperature sensitivity with respect to optical depth. Uncertainty in
500 the UV-B exposure response function, sensitivity of precipitation to temperature and uncertainty
501 in aerosol lifetime each contribute 1% or less to overall uncertainty in the result. When
502 calculating mortality due to PM_{2.5} and ozone individually, ERF uncertainty remains the greatest
503 contributor to overall variance, followed by uncertainty in the temperature sensitivity to optical
504 depth. However, this ordering is reversed for mortalities due to UV-B exposure. Furthermore,

505 application of an alternative ERF developed for global studies by Burnett et al (2014) results in
 506 mortality due to geoengineering-attributable PM_{2.5} falling by 22%. Mortalities calculated using
 507 several other ERFs are shown in the SI.

508 Table 3. Annual premature mortality impacts resulting from sulfate geoengineering sufficient to offset 1°C of surface warming.
 509 Mean outcomes are in bold, 95% intervals are shown in square brackets (N = 1,000). The 95% interval is calculated as the 2.5
 510 and 97.5th percentile values of the Monte Carlo simulation outcomes.

	Direct impacts		RF-driven impacts		All mechanisms
	Descending injection mass	Photochemical effects	Offset warming	Offset precipitation	
Surface ozone	-	-23,000 (-45,000 : -6,600)	-43,000 (-67,000 : -19,000)	-660 (-1,100 : -260)	-67,000 (-110,000 : -28,000)
PM _{2.5}	7,400 (2,300 : 16,000)	-1,400 (-2,400 : -520)	69,000 (41,000 : 95,000)	14,000 (7,100 : 21,000)	88,000 (53,000 : 120,000)
UV-B	-	4,100 (1,300 : 8,200)	400 (200 : 610)	-24 (-40 : -10)	4,500 (1,600 : 8,800)
All causes	7,400 (2,300 : 16,000)	-20,000 (-42,000 : -4,900)	26,000 (-12,000 : 63,000)	13,000 (6,600 : 20,000)	26,000 (-30,000 : 79,000)

511

512 All simulations were performed at a relatively coarse horizontal resolution (4°×5°). A
 513 2013 study indicated that while surface ozone exposure is insensitive to grid resolution, use of
 514 coarse horizontal resolution when calculating outcomes could result in mortality due to PM_{2.5}
 515 exposure being biased low by 30-40%. This is due to the covariance of peaks in PM_{2.5}
 516 concentration and population centers, which is not reflected at coarse resolution (*Punger et al.*,
 517 2013). However, changes in PM_{2.5} due to sulfate geoengineering are diffuse compared to modern
 518 anthropogenic PM_{2.5}, and this covariance is therefore likely to be reduced. These simulations
 519 also do not take into account the possible response of cloudiness to the increase in cloud
 520 condensation nuclei which could result from sulfate geoengineering, due to the descent of

521 emitted fine aerosol into the upper troposphere. In addition to potentially affecting the total
522 UV-B reaching the surface and the net RF associated with geoengineering (*Kuebbler et al.*,
523 2012), changes in cloudiness through this mechanism could affect surface precipitation and
524 thereby PM_{2.5} concentrations. Although outside the scope of this work, we consider assessment
525 of the response of cloudiness to be a priority for future research on surface-level impacts of
526 geoengineering.

527 These results must be weighed against the risks of climate change which sulfate
528 geoengineering seeks to mitigate, and the magnitude of current and future health impacts due to
529 degraded air quality. A study of the 2015 global burden of disease found that 4 million deaths
530 annually are attributable to degraded air quality, while air quality co-benefits of greenhouse gas
531 mitigation (including changes in precursor emissions) have been estimated at ~1.3 million fewer
532 mortalities per year in 2050 (*Cohen et al., 2017, West et al., 2013*). We find that the total air
533 quality and skin cancer related impacts of sulfate geoengineering sufficient to induce a 1°C
534 decrease in surface temperature are +26,000 (95% CI: -30,000 to +79,000) premature mortalities
535 per year. Normalizing by total population in 2040, this is equivalent to a change of +0.3 early
536 deaths per 100,000 population. For context, this can be compared to projected direct health
537 impacts of rising surface temperatures. A study of temperature-related mortality under a
538 “business as usual” (BAU) climate change scenario projected that a 3°C increase in average
539 surface temperature would result in an additional 63,000 mortalities per year in the US alone,
540 corresponding to +20 deaths per 100,000 population (*Deschênes et al., 2011*). These changes are
541 dominated by increased vulnerability during extreme cold and extreme heat events, resulting in
542 greater changes at higher baseline temperatures. Another study found that aggregate economic
543 impacts of temperature increases are approximately linear in temperature, and that BAU climate

544 change is estimated to reduce global average incomes by 23% within the next 80 years (*Burke et*
545 *al.*, 2015). These consequences of climate change must be weighed against the risks and benefits
546 of sulfate geoengineering, including (but not limited to) the impacts on air quality and UV
547 exposure explored in this study, which are relatively small and of uncertain sign.

548 **5 Conclusions**

549 We identify several mechanisms by which sulfate geoengineering may cause changes in
550 air quality and UV-B exposure, and we provide the first quantitative estimates of the impact of
551 sulfate geoengineering on global mortality rates from these causes. When sulfate geoengineering
552 is used to offset 1°C of temperature rise (or create 1°C cooling) we find that RF-driven impacts,
553 associated with offsetting the effects of climate change, result in a net increase in mortality,
554 while other (“direct”) impacts result in a net decrease. The net effect is an increase of 26,000
555 additional premature mortalities per year (95% interval: -30,000 to +79,000), although the
556 overall sign of the impact is uncertain. We find an 83% chance of a net increase in global
557 mortality due to air quality and UV-B exposure, with uncertainty in the exposure response
558 functions providing the greatest contribution to total uncertainty in the result.

559 Of the direct impact pathways considered, descent of injected sulfate aerosol from the
560 stratosphere is found to be a minor contributor to the overall impact of sulfate geoengineering.
561 The contribution of descending, injected aerosol to surface PM_{2.5} causes 7,400 additional
562 premature mortalities per year, compared to a decrease of 20,000 premature mortalities per year
563 resulting from the direct photochemical effects of sulfate geoengineering. This is made up of
564 4,100 additional skin cancer mortalities offset by 23,000 averted premature mortalities due to
565 decreased ozone exposure. By contrast, RF-driven impacts of sulfate geoengineering are found to
566 result in a net increase in mortality relative to the avoided future scenario. By offsetting 1°C of

567 atmospheric warming, greater concentrations of $PM_{2.5}$ are formed from existing emissions,
568 resulting in an additional 69,000 premature mortalities per year. The reduction in radiative
569 forcing also offsets some of the anticipated increase in precipitation associated with climate
570 change, with longer aerosol lifetimes incurring an additional 14,000 premature mortalities per
571 year. These effects are partially offset by 44,000 avoided mortalities per year from RF-driven
572 changes in ozone exposure. The specific magnitudes depend on the amount of warming which is
573 being offset. The impacts of larger or smaller amounts of can be approximated by scaling the
574 warming to our $1^{\circ}C$ value.

575 This analysis does not account for ecological and climate feedback effects related to
576 increased CO_2 , possible induced or suppressed cloudiness, or public health impacts beyond
577 changes in mortality due to air quality and UV-B exposure. Deschênes et al. (2011) found that,
578 under a business-as-usual scenario with $3^{\circ}C$ of warming in 2070-2099, the direct impact of
579 increased temperatures due to climate change would be 63,000 premature mortalities per year
580 from extreme temperatures in the United States alone. Burke et al. (2015) estimated that
581 aggregate economic impacts of climate change will reduce global average incomes by 23% in the
582 same period. Although beyond the scope of this paper, weighing the broader effects of mitigating
583 climate change against the air quality and UV-B impacts computed here would provide a more
584 complete understanding of the net benefits and risks of sulfate geoengineering.

585 **Appendix A: Assessment of response linearity**

586 Four additional simulations are conducted to test the validity of the assumption that
587 impacts will scale linearly with input. For impacts due to changes in temperature and
588 precipitation, we simulate perturbations which are 5 times smaller than the CanESM2 output and

589 8.6 times smaller than the “full” perturbations corresponding to a 0.98 K cooling. A 0.5 TgS/yr
590 injection rate, resulting in a 0.040 increase in stratospheric optical depth, was simulated to
591 determine impact linearity with respect to these quantities in isolation from meteorological
592 feedbacks. A full list is given in Table 4. Second order effects due to effect interaction (e.g.
593 between precipitation impacts and injected sulfates) are addressed in Appendix B. The output
594 metric shown is the total mortalities as calculated without accounting for uncertainty in climate
595 or exposure response variables.

596

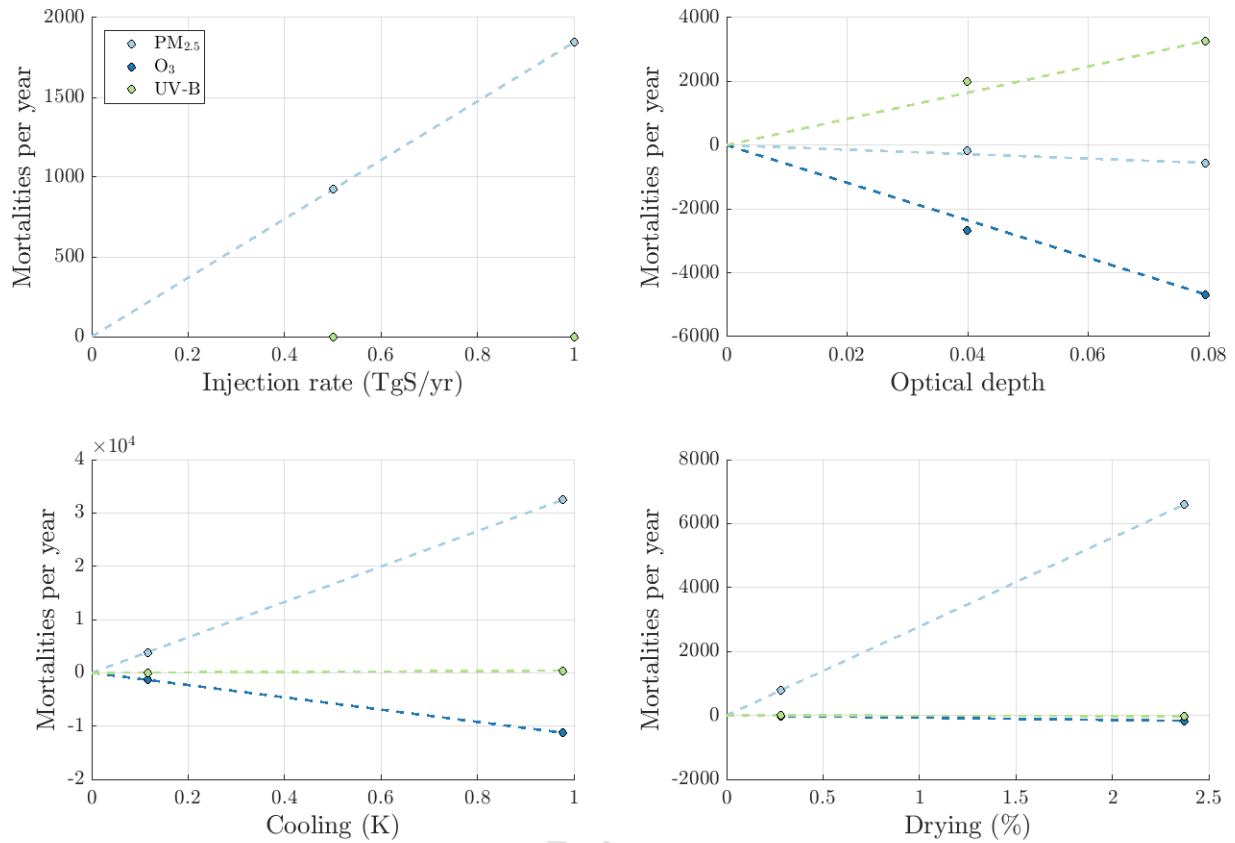
597 Table 4. Perturbation parameters used in simulations to establish response linearity.

Input	Small perturbation	Large perturbation
Injection rate (TgS/yr)	0.5	1.0
Optical depth (-)	0.040	0.079
Offset warming (K)	0.12	0.98
Offset precipitation (%)	0.28%	2.4%

598 The total mortalities calculated for each perturbation, broken down into those resulting
599 from exposure to PM_{2.5}, ozone and UV-B, are shown in Figure 3. Interpolation between zero and
600 the ‘full-scale’ perturbation shows a good agreement with the results of the smaller test
601 perturbation simulations. The exception to this is in the case of the response to an increase in
602 stratospheric aerosol optical depth $\Delta\tau$. For a $\Delta\tau$ of 0.040, the change in mortality due to skin
603 cancer is 21% greater than would be calculated by interpolation from the impact of a $\Delta\tau$ of
604 0.079, and the ozone reduction is 13% greater. The effect on PM_{2.5} exposure is negligible. This is
605 likely to be due to saturation, as reaction rates become limited by factors other than surface area
606 density of aerosol.

607

608



609

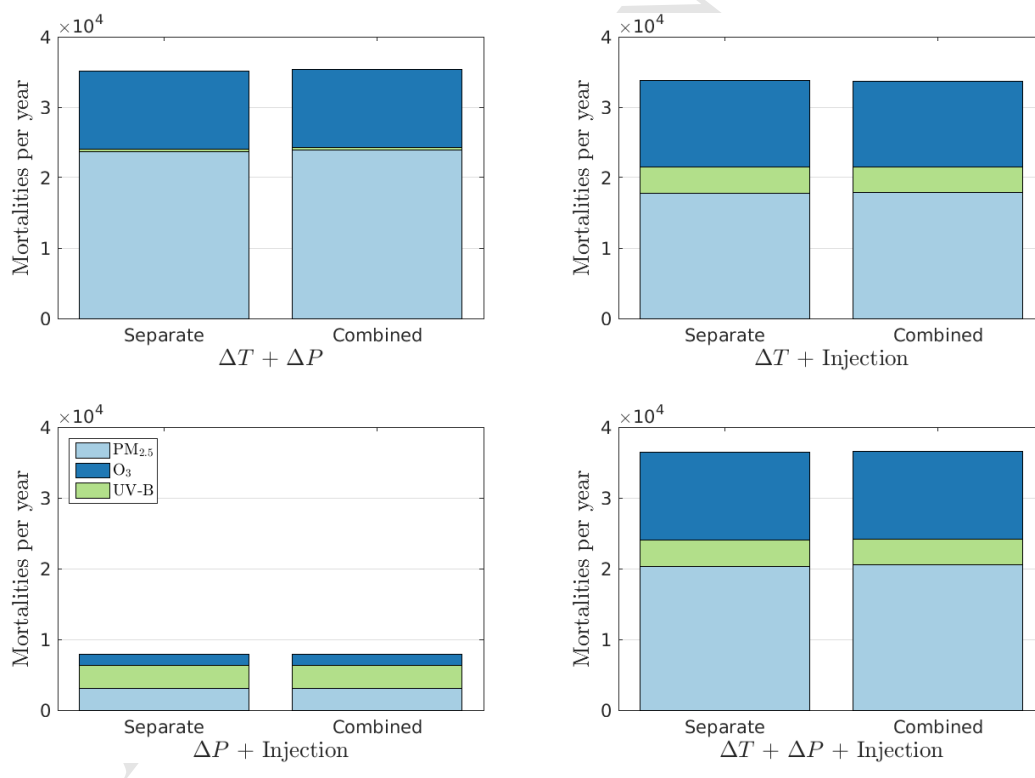
610 Figure 3. Response linearity with respect to each of the assessed mortality mechanisms. The dashed line represents the linear
 611 sensitivity used in each case when scaling calculated exposures for the purposes of uncertainty quantification.

612 Appendix B: Second-order sensitivities

613 Four additional simulations are conducted in which the inputs are combined to determine
 614 the effect of second order terms on the response. In the first three simulations, combinations of
 615 two parameters (temperature change, precipitation change, and injection rate) are changed
 616 simultaneously. In the final simulation, all three are modified together. For these simulations, the
 617 effect of descending aerosol and the photochemical effect of an increase in stratospheric optical
 618 depth are not separated.

619

620 The results of these simulations are shown in Figure 4. In each panel, the left-hand bar
 621 shows the total mortalities as calculated by linearly adding the exposure calculated by individual
 622 simulations, whereas the right-hand bar shows total mortalities as calculated using a single
 623 simulation in which the perturbations are simulated together. These estimates do not include
 624 uncertainty in climate variables. Inclusion of second-order effects changes the total calculated
 625 number of mortalities by less than $\pm 1\%$, suggesting that interaction between the three factors is
 626 not significant. However, this does not address possible meteorological feedbacks such as
 627 changes in cloud cover or ventilation.



628

629 Figure 4. Comparison of mortalities estimated by linear combination of calculated exposures from several perturbation
 630 simulations (left) and by direct simulation of multiple perturbations together (right). All totals agree to within $\pm 1\%$. Uncertainty
 631 in climate variables is not included in these estimates.

632 **Competing Interests**

633 The authors have no competing interests to declare.

634 **Funding sources**

635 This research did not receive any specific grant from funding agencies in the public, commercial,
636 or not-for-profit sectors.

637 **Acknowledgments, Samples, and Data**

638 All authors designed the research and wrote the paper. DKW undertook the
639 microphysical modeling. SDE undertook the GEOS-Chem modeling. The authors have no
640 financial conflicts of interest to declare.

641 We would like to acknowledge the work of Professor Christopher D. Holmes at Florida
642 State University, who implemented emissions of anthropogenic short-lived species in GEOS-
643 Chem based on the RCP scenarios and without whom this study would have taken significantly
644 longer. We acknowledge the World Climate Research Programme's Working Group on Coupled
645 Modelling, which is responsible for CMIP, and we thank the CanESM2 climate modeling group
646 for producing and making available their model output. For CMIP the U.S. Department of
647 Energy's Program for Climate Model Diagnosis and Intercomparison provides coordinating
648 support and led development of software infrastructure in partnership with the Global
649 Organization for Earth System Science Portals. We would also like to acknowledge Lorretta
650 Mickley and Lee Murray, for guidance regarding GEOS-Chem meteorology. Thanks to Jason
651 Cole of Environment Canada for supplying meteorological data from the climate model
652 CanESM2 produced as part of the GeoMIP and CMIP5 projects, and for assistance in its

653 interpretation. Thanks also to Ben Kravitz for co-ordinating the GeoMIP project and assisting in
654 acquiring and processing GeoMIP output from CanESM2 and the other climate models involved.
655 We also thank Arjan van Dijk for his help understanding specific skin cancer risks associated
656 with UV exposure. We acknowledge the Nimbus-7 mission scientists and associated NASA
657 personnel for the production of the data used in this research effort. In particular we would like
658 to thank Nickolay Krotkov for his assistance in converting UV-B to erythemal dose. The GEOS-
659 5.2.0 data used in this study/project have been provided by the Global Modeling and
660 Assimilation Office (GMAO) at NASA Goddard Space Flight Center.

661 Processed simulation output can be obtained from the corresponding author on request.
662 No new data were used in producing this manuscript.

663 **References**

- 664 Anenberg, S. C., Horowitz, L. W., Tong, D. Q., and West, J. J. (2010), An estimate of the global
665 burden of anthropogenic ozone and fine particulate matter on premature human mortality
666 using atmospheric modeling. *Environmental Health Perspectives*, 118(9), 1189–1195.
- 667 Benduhn, F., Schallock, J., and Lawrence, M. G. (2016), Early growth dynamical implications
668 for the steerability of stratospheric solar radiation management via sulfur aerosol
669 particles. *Geophysical Research Letters*, 43(18), 2016GL070701.
- 670 Burke, M., S. M. Hsiang, and E. Miguel (2015), Global non-linear effect of temperature on
671 economic production, *Nature*, (1), 1–16.
- 672 Barrett, S. R. H., Yim, S. H. L., Gilmore, C. K., Murray, L. T., Kuhn, S. R., Tai, A. P. K.,
673 Yantosca, R. M., Byun, D. W., Li, X., Levy, J., Ashok, A., Koo, J., Wong, H. M.,
674 Dessens, O., Balasubramanian, S., Fleming G. G., Malina, R., Pearlson, M. N.,

- 675 Arunachalam, S., Francis, S. (2012), Public Health, Climate and Economic Impacts of
676 Desulfurizing Jet Fuel, *Environ Sci Tech.*, 46(8), 4275–4282.
- 677 Bright, E. A., Rose, A. N., and Urban, M. L. (2012), LandScan 2012. Oak Ridge, TN: Oak Ridge
678 National Laboratory. Retrieved from <http://www.ornl.gov/landscan/>
- 679 Burnett, R.T., Pope, C.A., Ezzati, M., Olives, C., Lim, S.S., Mehta, S., Shin, H.H., Singh, G.,
680 Hubbell, B., Brauer, M., Anderson, H.R., Smith, K.R., Balmes, J.R., Bruce, N.G., Kan,
681 H., Laden, F., Prüss-Ustün, A., Turner, M.C., Gapstur, S.M., Diver, W.R., and Cohen, A.,
682 (2014), An integrated risk function for estimating the global burden of disease
683 attributable to ambient fine particulate matter exposure. *Environ. Health Perspect.* 122,
684 397–403.
- 685 Caiazzo, F., Ashok, A., Waitz, I. A., Yim, S. H. L., and Barrett, S. R. H. (2013), Air pollution
686 and early deaths in the United States. Part I: Quantifying the impact of major sectors in
687 2005. *Atmospheric Environment*, 79, 198–208.
- 688 Caldeira, K., Bala, G., and Cao, L. (2013), The Science of Geoengineering. *Annual Review of*
689 *Earth and Planetary Sciences*, 41(1), 231–256.
- 690 Carpenter, L.J., Reimann, S., Burkholder, J.B., Clerbaux, C., Hall, B.D., Hossaini, R., Laube,
691 J.C., and Yvon-Lewis, S.A. (2014), Ozone-Depleting Substances (ODSs) and Other
692 Gases of Interest to the Montreal Protocol. In *Scientific Assessment of Ozone Depletion:*
693 *2014*. Geneva, Switzerland: World Meteorological Organization.
- 694 Chen, J.-P., Tsai, I.-C., and Lin, Y.-C. (2013), A statistical–numerical aerosol parameterization
695 scheme. *Atmos. Chem. Phys.*, 13(20), 10483–10504.

- 696 Chylek, P., Li, J., Dubey, M. K., Wang, M., and Lesins, G. (2011), Observed and model
697 simulated 20th century Arctic temperature variability: Canadian Earth System Model
698 CanESM2. *Atmospheric Chemistry and Physics Discussions*, 11(8), 22893–22907.
- 699 Clarke, L., J. Edmonds, H. Jacoby, H. Pitcher, J. Reilly, and R. Richels (2007), Scenarios of
700 Greenhouse Gas Emissions and Atmospheric Concentrations. Sub-report 2.1A of
701 Synthesis and Assessment Product 2.1 by the U.S. Climate Change Science Program and
702 the Subcommittee on Global Change Research, Department of Energy, Office of
703 Biological & Environmental Research, Washington.
- 704 Cohen, A.J., Brauer, M., Burnett, R., Anderson, H.R., Frostad, J., Estep, K., Balakrishnan, K.,
705 Brunekreef, B., Dandona, L., Dandona, R., Feigin, V., Freedman, G., Hubbell, B.,
706 Jobling, A., Kan, H., Knibbs, L., Liu, Y., Martin, R., Morawska, L., Pope, C.A., 3rd,
707 Shin, H., Straif, K., Shaddick, G., Thomas, M., van Dingenen, R., van Donkelaar, A.,
708 Vos, T., Murray, C.J.L., Forouzanfar, M.H., (2017), Estimates and 25-year trends of the
709 global burden of disease attributable to ambient air pollution: an analysis of data from the
710 Global Burden of Diseases Study 2015. *Lancet* 389, 1907–1918.
- 711 Corbett, J. J., Winebrake, J. J., Green, E. H., Kasibhatla, P., Eyring, V., and Lauer, A. (2007),
712 Mortality from Ship Emissions: A Global Assessment. *Environ Sci Tech*, 41(24), 8512–
713 8518.
- 714 de Gruijl, F.R., and Van der Leun, J.C., (1994), Estimate of the wavelength dependency of
715 ultraviolet carcinogenesis in humans and its relevance to the risk assessment of a
716 stratospheric ozone depletion. *Health Phys.* 67, 319–325.

- 717 Deschênes, O., and M. Greenstone (2011), Climate Change, Mortality, and Adaptation: Evidence
718 from Annual Fluctuations in Weather in the U.S, *Am. Econ. J. Appl. Econ.*, 3(4), 152–
719 185.
- 720 Eastham, S. D., and S. R. H. Barrett (2016), Aviation-attributable ozone as a driver for changes
721 in mortality related to air quality and skin cancer, *Atmospheric Environment*, 144, 17-23.
- 722 Eastham, S. D., D. K. Weisenstein, and S. R. H. Barrett (2014), Development and evaluation of
723 the unified tropospheric–stratospheric chemistry extension (UCX) for the global
724 chemistry-transport model GEOS-Chem, *Atmos. Environ.*, 89, 52–63.
- 725 Effiong, U., and R. L. Neitzel (2016), Assessing the direct occupational and public health
726 impacts of solar radiation management with stratospheric aerosols, *Environ. Health*,
727 15(1), 7.
- 728 Fang, Y., Naik, V., Horowitz, L. W., and Mauzerall, D. L. (2013), Air pollution and associated
729 human mortality: the role of air pollutant emissions, climate change and methane
730 concentration increases from the preindustrial period to present. *Atmospheric Chemistry
731 and Physics*, 13(3), 1377–1394.
- 732 Fiore, A.M., Naik, V., Spracklen, D.V., Steiner, A., Unger, N., Prather, M., Bergmann, D.,
733 Cameron-Smith, P.J., Cionni, I., Collins, W.J., Dalsøren, S., Eyring, V., Folberth, G. a.,
734 Ginoux, P., Horowitz, L.W., Josse, B., Lamarque, J.-F., MacKenzie, I. a., Nagashima, T.,
735 O’Connor, F.M., Righi, M., Rumbold, S.T., Shindell, D.T., Skeie, R.B., Sudo, K., Szopa,
736 S., Takemura, and T., Zeng, G. (2012), Global air quality and climate, *Chem. Soc. Rev.*,
737 41, 6663.

- 738 Giorgi, F., and Francisco, R. (2000), Uncertainties in regional climate change prediction: a
739 regional analysis of ensemble simulations with the HADCM2 coupled AOGCM. *Climate*
740 *Dynamics*, 16, 169–182.
- 741 Guy, G. P., S. R. Machlin, D. U. Ekwueme, and K. R. Yabroff (2015), Prevalence and costs of
742 skin cancer treatment in the u.s., 2002-2006 and 2007-2011, *Am. J. Prev. Med.*, 48(2),
743 183–187.
- 744 Heckendorn, P., D. Weisenstein, S. Fueglistaler, B. P. Luo, E. Rozanov, M. Schraner, L. W.
745 Thomason, and T. Peter (2009), The impact of geoengineering aerosols on stratospheric
746 temperature and ozone, *Environ. Res. Lett.*, 4(4), 045108.
- 747 Hoek, G., R. M. Krishnan, R. Beelen, A. Peters, B. Ostro, B. Brunekreef, and J. D. Kaufman
748 (2013), Long-term air pollution exposure and cardio- respiratory mortality: a review,
749 *Environ. Health*, 12(1), 43.
- 750 Jacob, D. J., and Winner, D. a. (2009), Effect of climate change on air quality. *Atmospheric*
751 *Environment*, 43(1), 51–63.
- 752 Jerrett, M., R. T. Burnett, C. A. Pope, K. Ito, G. Thurston, D. Krewski, Y. Shi, E. Calle, and M.
753 Thun (2009), Long-term ozone exposure and mortality, *N. Engl. J. Med.*, 360(11), 1085–
754 1095.
- 755 Kirtman, B., Power, S.B., Adedoyin, J.A., Boer, G.J., Bojariu, R., Camilloni, I., Doblaz-Reyes,
756 F.J., Fiore, A.M., Kimoto, M., Meehl, G.A., Prather, M., Sarr, A., Schär, C., Sutton, R.,
757 van Oldenborgh, G.J., Vecchi, G., and Wang, H.J. (2014), Near-term climate change:
758 projections and predictability, in *Climate Change 2013: The Physical Science Basis*.
759 Contribution of Working Group I to the Fifth Assessment Report of the

- 760 Intergovernmental Panel on Climate Change, edited by T. F. Stocker, D. Qin, G.-K.
761 Plattner, M. Tignor, S. K. Allen, J. Boschung, A. Nauels, Y. Xia, V. Bex, and P. M.
762 Midgley, pp. 953–1028, Cambridge University Press, Cambridge.
- 763 Kravitz, B., A. Robock, P. M. Forster, J. M. Haywood, M. G. Lawrence, and H. Schmidt (2013),
764 An overview of the Geoengineering Model Intercomparison Project (GeoMIP), *J.*
765 *Geophys. Res. D: Atmos.*, 118(23), 13,103–113,107.
- 766 Kravitz, B., MacMartin, D.G., Robock, A., Rasch, P.J., Ricke, K.L., Cole, J.N.S., Curry, C.L.,
767 Irvine, P.J., Ji, D., Keith, D.W., Egill Kristjánsson, J., Moore, J.C., Muri, H., Singh, B.,
768 Tilmes, S., Watanabe, S., Yang, S., and Yoon, J.-H., (2014), A multi-model assessment
769 of regional climate disparities caused by solar geoengineering. *Environmental Research*
770 *Letters*, 9. <https://doi.org/10.1088/1748-9326/9/7/074013>
- 771 Krewski, D., Jerrett, M., Burnett, R.T., Ma, R., Hughes, E., Shi, Y., Turner, M.C., Pope, C.A.I.,
772 Thurston, G., Calle, E.E., and Thun, M.J., (2009), Extended follow-up and spatial
773 analysis of the American Cancer Society study linking particulate air pollution and
774 mortality. HEI Research Report 140, Health Effects Institute, Boston, MA.
- 775 Kuebbeler, M., Lohmann, U., Feichter, J., (2012), Effects of stratospheric sulfate aerosol geo-
776 engineering on cirrus clouds. *Geophys. Res. Lett.* 39.
- 777 Lelieveld, J., Barlas, C., Giannadaki, D., and Pozzer, A. (2013). Model calculated global,
778 regional and megacity premature mortality due to air pollution. *Atmospheric Chemistry*
779 *and Physics*, 13(14), 7023–7037.
- 780 Li, F., Stolarski, R. S., and Newman, P. A. (2009). Stratospheric ozone in the post-CFC era.
781 *Atmos. Chem. Phys.*.

782 Lim, S.S., Vos, T., Flaxman, A.D., Danaei, G., Shibuya, K., Adair-Rohani, H., Amann, M.,
783 Anderson, H.R., Andrews, K.G., Aryee, M., Atkinson, C., Bacchus, L.J., Bahalim, A.N.,
784 Balakrishnan, K., Balmes, J., Barker-Collo, S., Baxter, A., Bell, M.L., Blore, J.D., Blyth,
785 F., Bonner, C., Borges, G., Bourne, R., Boussinesq, M., Brauer, M., Brooks, P., Bruce,
786 N.G., Brunekreef, B., Bryan-Hancock, C., Bucello, C., Buchbinder, R., Bull, F., Burnett,
787 R.T., Byers, T.E., Calabria, B., Carapetis, J., Carnahan, E., Chafe, Z., Charlson, F., Chen,
788 H., Chen, J.S., Cheng, A.T.-A., Child, J.C., Cohen, A., Colson, K.E., Cowie, B.C., Darby,
789 S., Darling, S., Davis, A., Degenhardt, L., Dentener, F., Des Jarlais, D.C., Devries, K.,
790 Dherani, M., Ding, E.L., Dorsey, E.R., Driscoll, T., Edmond, K., Ali, S.E., Engell, R.E.,
791 Erwin, P.J., Fahimi, S., Falder, G., Farzadfar, F., Ferrari, A., Finucane, M.M., Flaxman,
792 S., Fowkes, F.G.R., Freedman, G., Freeman, M.K., Gakidou, E., Ghosh, S., Giovannucci,
793 E., Gmel, G., Graham, K., Grainger, R., Grant, B., Gunnell, D., Gutierrez, H.R., Hall, W.,
794 Hoek, H.W., Hogan, A., Hosgood, H.D., Hoy, D., Hu, H., Hubbell, B.J., Hutchings, S.J.,
795 Ibeanusi, S.E., Jacklyn, G.L., Jasrasaria, R., Jonas, J.B., Kan, H., Kanis, J. a., Kassebaum,
796 N., Kawakami, N., Khang, Y.-H., Khatibzadeh, S., Khoo, J.-P., Kok, C., Laden, F.,
797 Laloo, R., Lan, Q., Lathlean, T., Leasher, J.L., Leigh, J., Li, Y., Lin, J.K., Lipshultz,
798 S.E., London, S., Lozano, R., Lu, Y., Mak, J., Malekzadeh, R., Mallinger, L., Marcenes,
799 W., March, L., Marks, R., Martin, R., McGale, P., McGrath, J., Mehta, S., Mensah, G. a.,
800 Merriman, T.R., Micha, R., Michaud, C., Mishra, V., Mohd Hanafiah, K., Mokdad, A. a.,
801 Morawska, L., Mozaffarian, D., Murphy, T., Naghavi, M., Neal, B., Nelson, P.K., Nolla,
802 J.M., Norman, R., Olives, C., Omer, S.B., Orchard, J., Osborne, R., Ostro, B., Page, A.,
803 Pandey, K.D., Parry, C.D.H., Passmore, E., Patra, J., Pearce, N., Pelizzari, P.M., Petzold,
804 M., Phillips, M.R., Pope, D., Pope, C.A., Powles, J., Rao, M., Razavi, H., Rehfues, E. a.,

805 Rehm, J.T., Ritz, B., Rivara, F.P., Roberts, T., Robinson, C., Rodriguez-Portales, J. a.,
806 Romieu, I., Room, R., Rosenfeld, L.C., Roy, A., Rushton, L., Salomon, J. a., Sampson,
807 U., Sanchez-Riera, L., Sanman, E., Sapkota, A., Seedat, S., Shi, P., Shield, K., Shivakoti,
808 R., Singh, G.M., Sleet, D. a., Smith, E., Smith, K.R., Stapelberg, N.J.C., Steenland, K.,
809 Stöckl, H., Stovner, L.J., Straif, K., Straney, L., Thurston, G.D., Tran, J.H., Van
810 Dingenen, R., van Donkelaar, A., Veerman, J.L., Vijayakumar, L., Weintraub, R.,
811 Weissman, M.M., White, R. a., Whiteford, H., Wiersma, S.T., Wilkinson, J.D., Williams,
812 H.C., Williams, W., Wilson, N., Woolf, A.D., Yip, P., Zielinski, J.M., Lopez, A.D.,
813 Murray, C.J.L., Ezzati, M., AlMazroa, M. a., and Memish, Z. a. (2012), A comparative
814 risk assessment of burden of disease and injury attributable to 67 risk factors and risk
815 factor clusters in 21 regions, 1990-2010: a systematic analysis for the Global Burden of
816 Disease Study 2010. *The Lancet*, 380(9859), 2224–2260.

817 McCormick, M. P., L. W. Thomason, and C. R. Trepte (1995), Atmospheric effects of the Mt
818 Pinatubo eruption, *Nature*, 373, 399–404.

819 Niemeier, U., and Timmreck, C. (2015), What is the limit of climate engineering by stratospheric
820 injection of SO₂? *Atmos. Chem. Phys.*, 15(16), 9129–9141.

821 Nowack, P. J., N. L. Abraham, P. Braesicke, and J. A. Pyle (2016), Stratospheric ozone changes
822 under solar geoengineering : implications for UV exposure and air quality, *Atmos. Chem.*
823 *Phys.*, 16, 4191–4203.

824 Ostro, B., Prüss-Üstün, A., Campbell-Lendrum, D., Corvalán, C., and Woodward, A. (2004),
825 *Outdoor air pollution: Assessing the environmental burden of disease at national and*
826 *local levels*. Geneva, Switzerland: World Health Organization.

- 827 Pierce, J. R., D. K. Weisenstein, P. Heckendorn, T. Peter, and D. W. Keith (2010), Efficient
828 formation of stratospheric aerosol for climate engineering by emission of condensible
829 vapor from aircraft, *Geophys. Res. Lett.*, 37(18), doi:10.1029/2010GL043975.
- 830 Pitari, G., V. Aquila, and B. Kravitz (2014), Stratospheric ozone response to sulfate
831 geoengineering: Results from the Geoengineering Model Intercomparison Project
832 (GeoMIP), *Journal of Geophysical Research - Atmospheres*, (November 1991), 2629–
833 2653.
- 834 Pope, C. A., III, Burnett, R. T., Thun, M. J., Calle, E. E., Krewski, D., and Thurston, G. D.
835 (2002), Lung Cancer, Cardiopulmonary Mortality, and Long-term Exposure to Fine
836 Particulate Air Pollution. *Journal of the American Medical Association*, 287(9), 1132–
837 1141.
- 838 Pungler, E. M., and J. J. West (2013), The effect of grid resolution on estimates of the burden of
839 ozone and fine particulate matter on premature mortality in the USA, *Air Qual. Atmos.*
840 *Health*, 6(3), 563–573.
- 841 Rasch, P. J., P. J. Crutzen, and D. B. Coleman (2008), Exploring the geoengineering of climate
842 using stratospheric sulfate aerosols: The role of particle size, *Geophys. Res. Lett.*, 35(2),
843 1–6.
- 844 Reilly, J., Hohmann, N., Kane, S. (1994), Climate change and agricultural trade: Who benefits,
845 who loses? *Glob. Environ. Change* 4, 24–36.
- 846 Saltelli, A., M. Ratto, T. Andres, F. Campolongo, J. Cariboni, D. Gatelli, M. Saisana, and S.
847 Tarantola (2008), *Global Sensitivity Analysis: The Primer*, Wiley.

- 848 Silva, R.A., West, J.J., Zhang, Y., Anenberg, S.C., Lamarque, J.-F., Shindell, D.T., Collins, W.J.,
849 Dalsoren, S., Faluvegi, G., Folberth, G., Horowitz, L.W., Nagashima, T., Naik, V.,
850 Rumbold, S., Skeie, R., Sudo, K., Takemura, T., Bergmann, D., Cameron-Smith, P.,
851 Cionni, I., Doherty, R.M., Eyring, V., Josse, B., MacKenzie, I. a., Plummer, D., Righi,
852 M., Stevenson, D.S., Strode, S., Szopa, S., and Zeng, G. (2013), Global premature
853 mortality due to anthropogenic outdoor air pollution and the contribution of past climate
854 change. *Environmental Research Letters: ERL [Web Site]*, 8(3), 034005.
- 855 Slaper, H., G. J. Velders, J. S. Daniel, F. R. de Gruijl, and J. C. van der Leun (1996), Estimates
856 of ozone depletion and skin cancer incidence to examine the Vienna Convention
857 achievements, *Nature*, 384(6606), 256–258.
- 858 Smith, S.J., Aardenne, J. van, Klimont, Z., Andres, R.J., Volke, A., and Delgado Arias, S.,
859 (2011), Anthropogenic sulfur dioxide emissions: 1850–2005. *Atmos. Chem. Phys.* 11,
860 1101–1116.
- 861 Smith, S. J., and T. M. L. Wigley (2006), Multi-Gas Forcing Stabilization with MiniCAM,
862 *Energy J.*, (Special Issue #3), 373–391.
- 863 Tilmes, S., R. R. Garcia, D. E. Kinnison, A. Gettelman, and P. J. Rasch (2009), Impact of
864 geoengineered aerosols on the troposphere and stratosphere, *J. Geophys. Res.*, 114(D12),
865 D12305.
- 866 Tilmes, S., D. E. Kinnison, R. R. Garcia, R. Salawitch, T. Canty, J. Lee-Taylor, S. Madronich,
867 and K. Chance (2012), Impact of very short-lived halogens on stratospheric ozone
868 abundance and UV radiation in a geo-engineered atmosphere, *Atmos. Chem. Phys.*, 12,
869 10945–10955.

- 870 World Health Organization (2014), *Burden of disease from Household and Ambient Air*
871 *Pollution for 2012*, World Health Organization, Geneva.
- 872 United Nations Department of Economic and Social Affairs (Population Division) (2013), World
873 *Population Prospects: The 2012 revision*,
- 874 United States National Academy of Sciences (NAS). Geoengineering. (1992). In *Policy*
875 *Implications of Greenhouse Warming: mitigation, adaptation, and the science base*.
- 876 van Dijk, A., Slaper, H., den Outer, P.N., Morgenstern, O., Braesicke, P., Pyle, J. a., Garny, H.,
877 Stenke, A., Dameris, M., Kazantzidis, A., Tourpali, K., and Bais, A.F., (2013), Skin
878 cancer risks avoided by the Montreal Protocol--worldwide modeling integrating coupled
879 climate-chemistry models with a risk model for UV. *Photochemistry and Photobiology*,
880 89(1), 234–246.
- 881 Weisenstein, D. K., G. K. Yue, M. K. W. Ko, N.-D. Sze, J. M. Rodriguez, and C. J. Scott (1997),
882 A two-dimensional model of sulfur species and aerosols, *J. Geophys. Res.*, 102(97).
- 883 Weisenstein, D. K., J. E. Penner, M. Herzog, and X. Liu (2007), Global 2-D intercomparison of
884 sectional and modal aerosol modules, *Atmos. Chem. Phys.*.
- 885 West, J.J., Smith, S.J., Silva, R.A., Naik, V., Zhang, Y., Adelman, Z., Fry, M.M., Anenberg, S.,
886 Horowitz, L.W., Lamarque, J.-F., (2013), Co-benefits of Global Greenhouse Gas
887 Mitigation for Future Air Quality and Human Health. *Nat. Clim. Chang.* 3, 885–889.
- 888 Wild, O., Zhu, X., and Prather, M. J. (2000), Fast-J: Accurate simulation of in- and below-cloud
889 photolysis in tropospheric chemical models. *Journal of Atmospheric Chemistry*, (37),
890 245–282.

- 891 Wise, M., K. Calvin, A. Thomson, L. Clarke, B. Bond-Lamberty, R. Sands, S. J. Smith, A.
892 Janetos, and J. Edmonds (2009), Implications of limiting CO₂ concentrations for land use
893 and energy, *Science*, 324(5931), 1183–1186.
- 894 Xia, L., Nowack, P. J., Tilmes, S., and Robock, A. (2017), Impacts of stratospheric sulfate
895 geoengineering on tropospheric ozone. *Atmospheric Chemistry and Physics*, 17(19),
896 11913–11928.
- 897 Zhang, H., S. Wu, Y. Huang, and Y. Wang (2014), Effects of stratospheric ozone recovery on
898 photochemistry and ozone air quality in the troposphere, *Atmos. Chem. Phys.*, 14, 4079–
899 4086.